6

Electrospun Metallic Nanofibers Fabricated by Electrospinning and Metallization

Kai Wei, Hae-Rim Kim, Byoung-Suhk Kim and Ick-Soo Kim
Faculty of Textile Science and Technology, Shinshu University, Japan

1. Introduction

The development of high value added one-dimensional (1D) electrospun nanofibers and structures (such as wires, belts and tubes) have tremendously increased over the last decade. Today, a wide variety of nano-objects (such as metal nanoparticles,[1–3] clays,[4] carbon nanotubes,[5, 6] ceramics,[7] etc.) can be immobilized onto nanofibers, which bring new materials' properties and potential applications in a broad range of areas such as electronics, medicine, sensor, and controlled release technology. As a result, a tremendous amount of effort has been devoted to the synthesis, characterization and utilization of nanofibers composites with well-controlled dimensions and properties. Indeed, extensive research and development in the 21st century is directed towards the development of novel hybrid nanomaterials with tunable properties. The purpose of such formulations is to achieve unique and superior properties that can not be achieved using only a single component of the hybrids. In this way, one can combine the properties of an organic component (polymers, biomolecules) such as mechanical toughness and flexibility with the hardness and thermal stability of the inorganic component (carbon, metals, ceramics, and glass) into a single system.[8,9] The new nanofibrous products based on the immobilization of functional nanomaterials onto electrospun nanofibers have recently attracted significant attention from both the academic and industrial sectors.[10–12] The main strategies for developing new nanostructured nanofibers were mostly carried out by direct electrostatic spinning of various polymers with molecular building blocks or polymer solutions (or polymer melts) with well-dispersed nano-objects,[1–7] and by co-electrospinning core–shell polymer nanofiber using a single-nozzle technique,[13,14] and by mimicking natural self-assembled process to produce hierarchically ordered self-assembled nanofibers.[15]

This chapter concentrates on metallized nanofibers which can be serving as the necessary functional components in building nanoelectronics. Nanofibers with uniform diameters represent an ideal model system to fabricate metal nanofibers. Long polymer fibers with sub-micrometer diameters down to a few nanometers can be prepared by electrospinning, which is a process where polymer solutions or polymer melts are processed in an electrical field.[16, 17] Electrospun nanofiber has a history of more than 70 years. In 1934, Formhals patented his first invention relating to the process and the apparatus for producing artificial filaments using electric charge.[18] This technique involves the use of a high voltage to charge the surface of a polymer solution (or melt) droplet and thus to induce the ejection of a liquid jet through a capillary spinneret. From then, this technique had gradually received

more and more attention to prepare nanosized polymer fibers. Nanofibers produced by electrospinning are of industrial and scientific interest due to their long lengths, small diameters and pores, and high surface area per unit volume which enable them have enormous applications in tissue scaffolds, protective clothing, filtration, and sensors, etc. Numerous polymer systems, including homopolymers, various kinds of copolymers, blends, and composites were successfully electrospun.[16, 19-21] Besides lots of efforts for developing these new nanofibers, tailoring the surface chemistry and function of electrospun nanofibers is also of utmost importance for the application of these materials: for example, modification of surface properties such as chemical composition, functionality, and charge as well as biocompatibility is essential for the utilization of the resulting nanofibers in specific applications. Recent studies by several groups have demonstrated the potential use of metal nanofibers as active components in fabricating nanoscale devices. For instance, Yang et al.[22] reported the electrospinning of ultrafine poly(acrylonitrile) (PAN) fibers containing Ag nanoparticles. Then many other metal nanoparticles such as gold, titanium, copper have been successfully dispersed on into a variety of polymer nanofibers via electrospinning. Kumar and co-workers[23] reported the fabrication of novel metal oxide-coated polymeric nanofibers using the electrospinning and solution dipping technique. Greiner and co-workers[24] reported that the coating of the template and the formation of the walls of the tubes could be achieved by chemical vapor deposition (CVD) with poly (p-xylylene) (PPX) via a template route. Parsons and co-workers[25] recently employed atomic layer deposition (ALD) on electrospun polymer fibers as a direct means by which to construct inorganic microtubes with well-defined nanoscale walls composed of Al_2O_3 after the removal of the templating polymer. In addition, noble metal nanofibers (such as Ag and Au) exhibit strong absorption in the visible and near infrared regions, an optical feature substantially different from those of planar metal surface or bulk materials. However, most of the methods are very time-consuming. To overcome these disadvantages, it is necessary to find a reliable and straightforward method to produce a variety of the nanostructured nanofibers with controlled morphologies and microstructures. The conductive surface is often required for applications such as anti-static, conductive shield, packing, and protective materials. The metallic nanostructured nanofibers have a great potential for a wide range of applications in many industries. In this chapter, we introduce a straight forward combined technology of electrostatic spinning and metallization for producing the conductive nanostructured hybrid nanofiber webs. Such metalizing technology can be widely used to deposit very thin films on various substrates for commercial and scientific purposes. The morphologies, microstructures and mechanical properties of the resulting metallized nanofibers were characterized by field emission scanning electron microscopy (FE-SEM), X-ray diffraction (XRD) and tensile tester, respectively. The ability to deposit well-controlled coatings onto the nanofibers would expand the application of nanofibers, for instance electromagnetic interference shielding effectiveness (EMI SE), based on changes to both the physical and chemical properties of the nanofibers.

2. Experimental procedure

2.1 Materials

The polyurethane (PU, ca. 14 wt%) stock solution, which is currently used for mass production electrospinning, was kindly provided by TECHNOS Co., Ltd., Japan and used for

electrospinning.[26,27] Poly(vinyl alcohol) (PVA) (degree of hydrolysis = 88%, degree of polymerization (DP) ≈ 1,700) was obtained from Kuraray Co. Ltd., Japan. High purity aluminum (99.5%, grains 3-5 mm), tin (99.99%, grains 2-3 mm), copper (99.99%, wire-cut) and nickel (99.9% up, grains 2-5 mm) were purchased from Kojundo Chemical Laboratory Co., Ltd., Japan. All chemicals were of analytical grade and used without further purification.

2.2 Electrospinning

In order to produce electrospun nanofibers,[28-30] a high-voltage power supply (Har-100*12, Matsusada, Co., Japan) was used as the source of the electric field. The PVA was dissolved in distilled water, and the concentration of PVA solution was 12 wt%. Each polymer (PU and PVA) solution was supplied through a plastic syringe attached to a capillary tip with an inner diameter of 0.6 mm. The copper wire connected to a positive electrode (anode) was inserted into the polymer solution, and a negative electrode (cathode) was attached to a metallic collector (Fig. 1a). The voltage was controlled at the range of 8-12 kV. The distance between the capillary tip and the collector was fixed to be 15 cm. All solutions were electrospun onto a rotating metallic collector at room temperature under identical conditions.

2.3 Metallization

A system UEP-6000 (ULVAC, Inc., Japan) was used to deposit a metallic layer onto the organic nanofibers. A high-purity target metal was mounted on the vapor plate (Fig. 1b), and the nanofiber webs were fixed on the rotating holder with a side facing the target. The vacuum pressure was set at 2.0×10^{-3} Pa, the power was set at 10 kV, 270 mA. The deposition rate of the metallic layer was controlled to be about 1.0 Å/s (copper, thin deposition) and 0.2 Å/s (nickel deposition), respectively. The distance between the target and substrates was 400 mm. The thicknesses of metal layers were scanned by a coated thickness measurement with X-ray spectrometers (Fischerscope X-RAY XDL-B, Fischer Technology Inc., Germany).

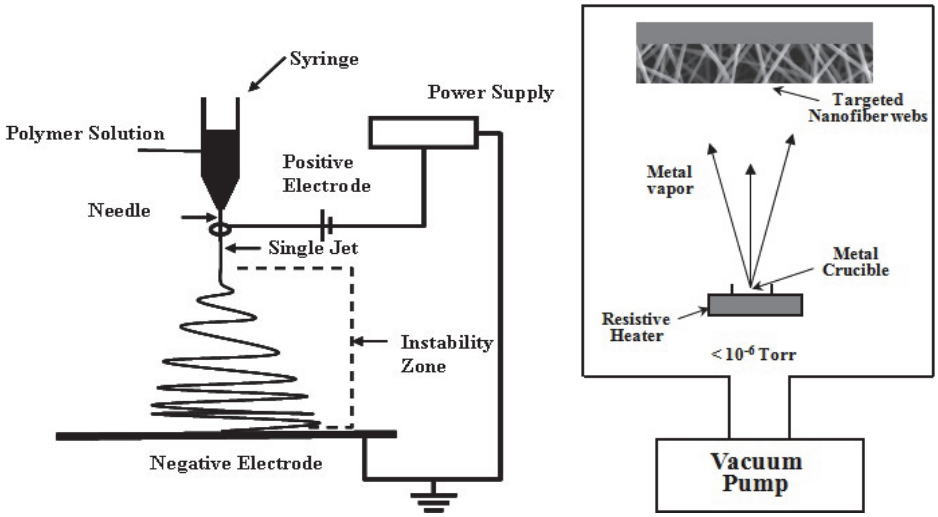

Fig. 1. Schematic of (a) electrospinning apparatus and (b) metallization.

2.4 Annealing process

After the Cu/Ni metal depositions, in order to produce the alloy nanofibers, the obtained Cu/Ni metal-deposited nanofibers were placed into the alundum crucible, and annealed in the electric furnace under N_2. Annealing process was conducted at various annealing temperatures and times, which were varied at the ranges of 250 ~ 600 ^oC and 6 ~ 24 hr, respectively. The heating rate was 5.0 ^oC/min.

2.5 Characterization

The morphologies of metallized nanofibers were characterized by field emission scanning electron microscope (FE-SEM) (Hitachi model S-5000). Wide angle X-ray diffraction (WAXD) experiments were carried out with a fixed anode X-ray generator operating at 40 kV and 150 mA (Rotaflex RTP300, Rigaku Co., Japan). The mechanical behaviors of metallized hybrid nanofiber webs were determined by a universal testing machine (TENSILON RTC1250A, A&D Company Ltd, Japan) under a crosshead speed 10mm/min at room temperature. In accordance with ASTM D-638, samples were prepared in the form of a dumbbell-shape and, then, at least five specimens were tested for tensile behavior and the averaged values were reported. For determining the tensile strength of metal deposited single nanofibers, we specially developed the test machine (FITRON NFR-1000, RHESCA Co., Japan). Three parameters were determined from each stress-strain curve: Young' modulus, tensile strength, and elongation at break. Elastic modulus or Young's modulus is the initial slope of the stress-strain curve. Tensile strength is the stress at failure and the strain corresponding to the tensile strength is the failure strain. The electrical volume resistivity ρ of the metallized hybrid nanofiber webs was measured using a standard four-point probe method at ambient conditions. The electrical volume resistivity ρ was calculated by Ohm's law, $\rho = (V/I)(wt/l)$, where V is voltage, I is current, l is distance between inside electrodes, w,t is width and thickness of the specimen, respectively. The shielding effect (SE) of the metalized nanofiber webs was analyzed using near-field antenna measurement systems, which consisted of a vector network analyzer (37169A Anritsu Co., Ltd.) and a near-field antenna measurement instrument (Tokai-techno Co., Ltd.) with a transmitting horn antenna and a receiving waveguide probe. The horn antenna and waveguide probe will be changed according to the frequency range to be measured.

3. Morphologies and microstructures of metallized nanofibers

3.1 Morphologies of metallized PU nanofibers

Fig. 2 shows typical FE-SEM micrographs of the pure PU and the metallized hybrid PU nanofiber webs with different thicknesses of the copper layer. As expected, electrospun nanofibers are deposited as a randomly oriented nanofiber web, forming a highly porous structure, which is held together by connecting sites such as crossing and bonding between the fibers. [31–33] The image at higher magnification (inset in Fig. 2a) shows that the surface morphology of pure PU nanofiber is smooth and uniform, with an average diameter of ca. 500 nm. On the other hand, after metallizing of pure PU nanofiber webs, the surface of metalized hybrid PU nanofibers becomes slightly coarse and looks rough (inset in Fig. 2b). When the thickness of the copper layer increases to 50 nm, it can be clearly seen that the tiny copper nanoparticles are formed through the surface of the nanofibers (inset in Fig. 2c); such nanoparticle becomes evident gradually with increase in the thickness of the copper layer

(inset in Fig. 2d). The results suggest that the metallic coppers are well deposited on the surface of nanofibers. In addition, the fibrous morphologies were satisfactorily conserved even after removal of the nanofiber template (by heat treatment at 400 ºC for 24 hr. The complete removal of the organic components was confirmed by FT-IR analysis) in the metallized hybrid PU nanofiber webs, indicating the successful deposition of metals on the surface of the nanofiber template. Furthermore, in the case of FE-SEM images in Fig. 2d (inset), nearly spherical copper nanoparticles were observed, with an average diameter of ca. 23 nm. This result is also well coincident with the results of WXAD, which will be explained below. The shape of copper nanoparticles is irregular and non-spherical, which may be attributed to the massive copper migration and aggregation. The migration and aggregation of copper nanoparticles are probably driven mostly by the instability of copper atoms due to their high surface free energy. [34] Therefore, the aggregation would produce thermodynamically stable particles with bigger sizes.

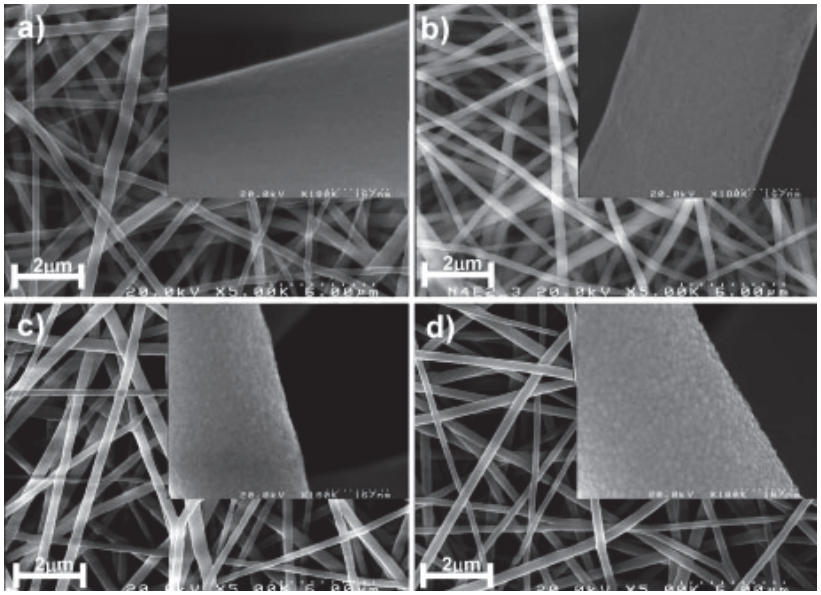

Fig. 2. FE-SEM photographs of pure PU (a) and metallized hybrid PU nanofiber webs with different copper layers of 10 nm (b), 50 nm (c), and 100 nm (d). Insets show FE-SEM images of each nanofibrous webs at higher magnification.

Fig. 3 shows the WAXD patterns of pure PU and metallized PU nanofibers. As seen in Fig. 3a, it was observed that the PU nanofibers have an amorphous structure. Moreover, the metallized PU nanofibers with the copper layer of 10 nm are also amorphous (Fig. 3b), suggesting that there is no formation of clear copper nanocrystals on the PU nanofibers, while the metallized PU nanofibers with the copper layer of 50 and 100 nm shows clearly typical crystalline peaks (Figs. 3c and 3d). The three peaks are observed at 2θ=43.5°, 50.0°and 73.5°, corresponding to the XRD peaks of crystalline copper and show that the copper crystals are in the form of (111), (200), and (220) reflections, [35] respectively. Furthermore, the full width at half-maximum (FWHM) of the strongest characteristic peak

(111) is used to estimate the average crystallite size by applying the following Debye – Scherrer equation, $D=\kappa\lambda/\beta\cos\theta$, where X-ray wavelength λ is 1.5402, κ is the shape factor which is often assigned a value of 0.89 if the shape is unknown, D is the average diameter of the crystals in angstroms, θ is the Bragg angle in degrees, and β is the full width at half-maximum of the strongest characteristic peak in radians. It was found that the averaged sizes of copper nanoparticles deposited on the PU nanofibers are ca. 12 and 23 nm for the metallized PU nanofibers with the copper layers of 50 and 100 nm, respectively. These results also agree well with FE-SEM data (FE-SEM images in Figs. 2c and 2d), indicating that spherical copper nanoparticles are observed.

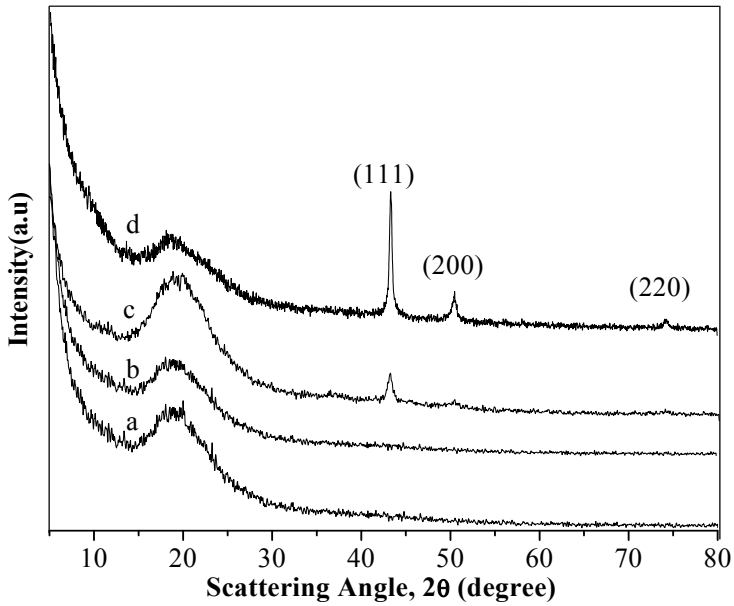

Fig. 3. X-ray diffraction patterns of pure PU nanofiber (a) and metalized hybrid PU nanofibers with different copper layers of 10 nm (b), 50 nm (c), and 100 nm (d).

3.2 Morphologies of metallic nanotubes

Fig. 4 shows typical FE-SEM micrographs of pure metallic nanotubes and nanofibers (a: 200 nm Cu-coated onto the nanofiber with the diameter of 200 – 250 nm, b: 200 nm Cu-coated onto the nanofiber with the diameter of 150 – 200 nm, c: 50 nm Cu-coated onto both side of the nanofiber with the diameter of 200 – 250 nm) after calcination at 400 ^{o}C for 24h, respectively. As seen in Fig. 4, pure metallic nanotubes exhibited a rough surface morphology compared to the metallized PVA nanofibers before calcination. The diameter of nanopores were found to be about 100 – 150 nm. On the other hand, the long metallic nanotubes were not obtained presumably due to incomplete coating of the metal layers onto the nanofiber template, but rather broken metallic nanotubes were observed (Fig. 4a). Therefore, in order to achieve complete metallic coverage of the nanofibers, the metallic coating onto both sides of the nanofibers were performed, and followed the removal of the nanofiber template to produce the long metallic nanotubes. The result is shown in Fig. 4c.

Clearly, it was observed that the long metallic nanotubes were successfully achieved without any breakages in pure metallic nanotubes. The formation of metallic nanotubes was also confirmed by transmission electron microscopy (TEM) analysis (data not shown). In addition, in order to investigate the diameter effect of the nanofibers on metallization, the electrospun PVA nanofibers with the smaller diameter ranging from 150 to 200 nm (PVA polymer solution: 8 – 10 wt%) were used and explored. Fig. 4b shows typical SEM images of pure metallic nanofibers. Interestingly, unusual pearl-necklace-like morphology was observed, which is not clear yet and at present. As a result, we could successfully prepare the pure metallic nanotubes or nanofibers depending on the diameter of the nanofibers and the thickness of deposited metal layer by using the combined technology of electrospinning and metallization.

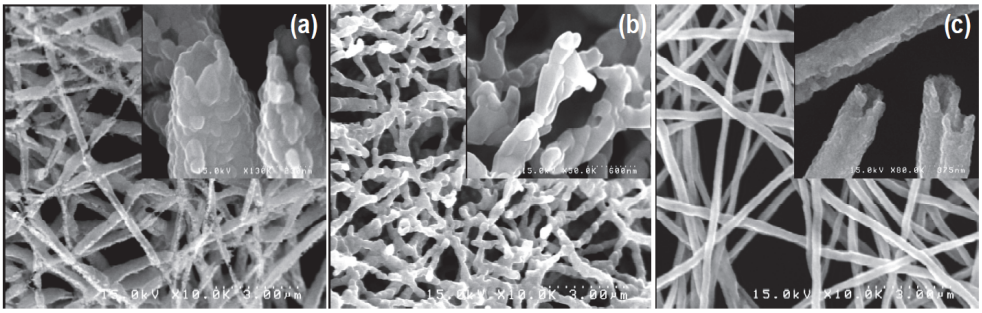

Fig. 4. FE-SEM micrographs of pure metallic nanotubes and nanofibers after calcination at 400 °C for 24h, respectively (a: 200 nm Cu-coated onto the nanofiber with the diameter of 200 – 250 nm, b: 200 nm Cu-coated onto the nanofiber with the diameter of 150 – 200 nm, c: 50 nm Cu-coated onto both side of the nanofiber with the diameter of 200 – 250 nm).

3.3 Metal alloy nanofibers

Metal alloy has been attracted considerable attention to metallurgists, materials engineers, and materials scientists in four major areas: (i) development of new alloys for specific applications; (ii) fabrication of these alloys into useful configurations; (iii) design and control of heat treatment procedures for specific alloys that will produce the required mechanical, physical, and chemical properties; and (iv) solving problems that arise with specific alloys in their performance in commercial applications, thus improving product predictability. In general, the use of phase diagrams is useful and allows research, development, and production to be done more efficiently and cost effectively. In the area of alloy development, phase diagrams have proved invaluable for tailoring existing alloys to avoid overdesign in current applications, designing improved alloys for existing and new applications, designing special alloys for special applications, and developing alternative alloys or alloys with substitute alloying elements to replace those containing scarce, expensive, hazardous, or ''critical'' alloying elements.[36] For instance, copper and nickel are completely soluble in all proportions in the solid state. Here, we attempt to study the annealing conditions for achieving the Cu/Ni metallized nanofibers from metal-deposited electrospun nanofibers prepared by electrospinning and metallization. Various annealing conditions, such as annealing temperature and time, and composition ratio of two metals (Cu and Ni) are investigated in order to find out optimum annealing process for the formation of alloy

nanofibers. We chose two different conditions with composition ratio of Cu/Ni 90:10 and 40:60 in deposited thickness, and investigated the morphologies and crystal structures of metal-deposited nanofibers before and after annealing. The annealing conditions, such as annealing temperatures and times were varied to find out optimum annealing process for the formation of alloy nanofibers.

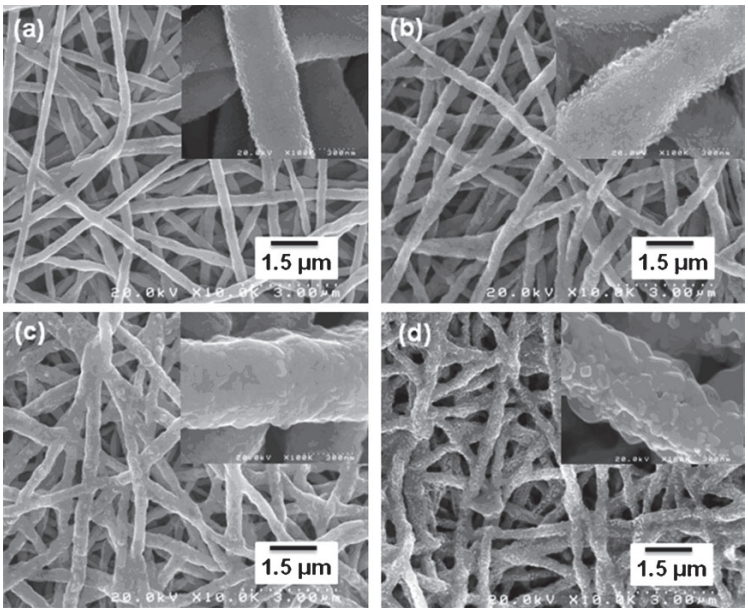

Fig. 5. FE-SEM images of Cu/Ni metallized (9:1, in deposition thickness) nanofibers before annealing (a) and after annealing at 250 °C (b), 400 °C (c), and 600 °C (d) for 12 h.

Fig. 5 shows FE-SEM images of Cu/Ni metallized (9:1, in deposition thickness) nanofibers before annealing (a) and after annealing at 250 °C (b), 400 °C (c), and 600 °C (d) for 12 h. It was found that the fibrous morphologies were satisfactorily conserved even after removal of the nanofiber template through an annealing process,[37] suggesting the successful deposition of metallic layers onto the surface of nanofiber template. As seen in Fig. 5, before annealing the surface of metal-deposited nanofibers exhibited a rough surface morphology due to the formation of the metallic granular nanoparticles (ca. 23 nm), whereas the surface roughness of the pure nanofibers was smooth (not shown). Moreover, the surface roughness of the metallized nanofibers annealed above 400 °C showed larger and irregular-shaped metal particles during annealing at higher temperature. On the other hand, the metallized nanofibers annealed at 250 °C exhibited the similar morphologies to the metal-deposited nanofibers before annealing, but irregular diameter with a node-structure, probably due to the partly flowing and deterioration of the viscoelastic polymer nanofiber around 250 °C.
Fig. 6 shows FE-SEM images of Cu/Ni metallized (4:6, in deposition thickness) nanofibers before annealing (a) and after annealing at 250 °C (b), 400 °C (c), and 600 °C (d) for 12 h. The similar annealing behavior was also observed at the composition ratio of Cu/Ni.40:60. That is, the surface roughness of Cu/Ni metallized nanofibers annealed at various temperatures for 12 h became coarse and rough as increasing the aging temperature.

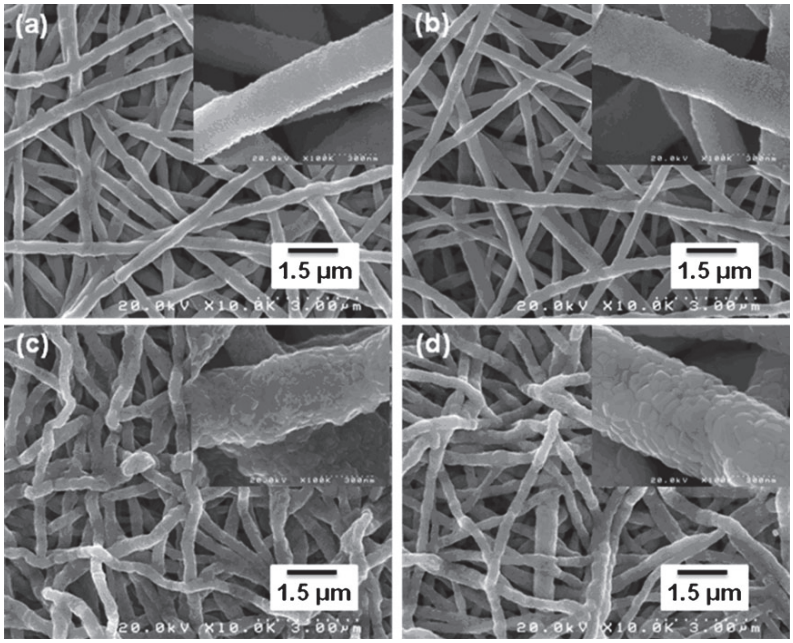

Fig. 6. FE-SEM images of Cu/Ni metallized (4:6, in deposition thickness) nanofibers before annealing (a) and after annealing at 250 °C (b), 400 °C (c), and 600 °C (d) for 12 h.

Fig. 7 shows FE-SEM images of Cu/Ni metallized (9:1, in deposition thickness) nanofibers annealed at 400 °C for (a, b) 6 h, (c, d) 12 h, and (e, f) 24 h, respectively. As seen in FE-SEM images at higher magnification (Figs. 7b, 7d and 7f), the irregular-shaped and different sized metal nanoparticles were observed. Moreover, it seemed that the irregular-shaped nanoparticles were converged gradually and its size became larger as increasing the annealing time, which may be attributed to the massive copper migration and aggregation during annealing at higher temperature. The migration and aggregation of metal nanoparticles are probably driven mostly by the instability of metal atoms due to their high surface free energy, and therefore would produce thermodynamically stable particles with bigger sizes.[20] As a result, these micrographs showed that sintering was occurred as increasing the annealing time at 400 °C, which was demonstrated by the variation in crystallite size during annealing, as confirmed by FE-SEM analysis. The result is well in accordance with the previously reported paper.[37]

3.4 Microstructures of Cu/Ni metallized nanofibers

Fig. 8 shows WAXD patterns of Cu/Ni metallized (9:1, in deposited thickness) nanofibers before annealing (a) and after annealing at 250 °C (b), 400 °C (c), and 600 °C (d) for 12 h. It was observed that the PU nanofibers had an amorphous structure, whereas the Cu/Ni deposited nanofibers before annealing clearly showed typical crystalline peaks of each pure metal, as seen in Fig. 8a. The typical crystalline peaks of both Cu and Ni metals were observed at 2θ = 43.6, 50.1, and 73.7, corresponding to the (111), (200), and (220) reflections, for pure Cu crystals[38] and at 2θ = 44.5, 51.9, and 76.6, corresponding to the (111), (200),

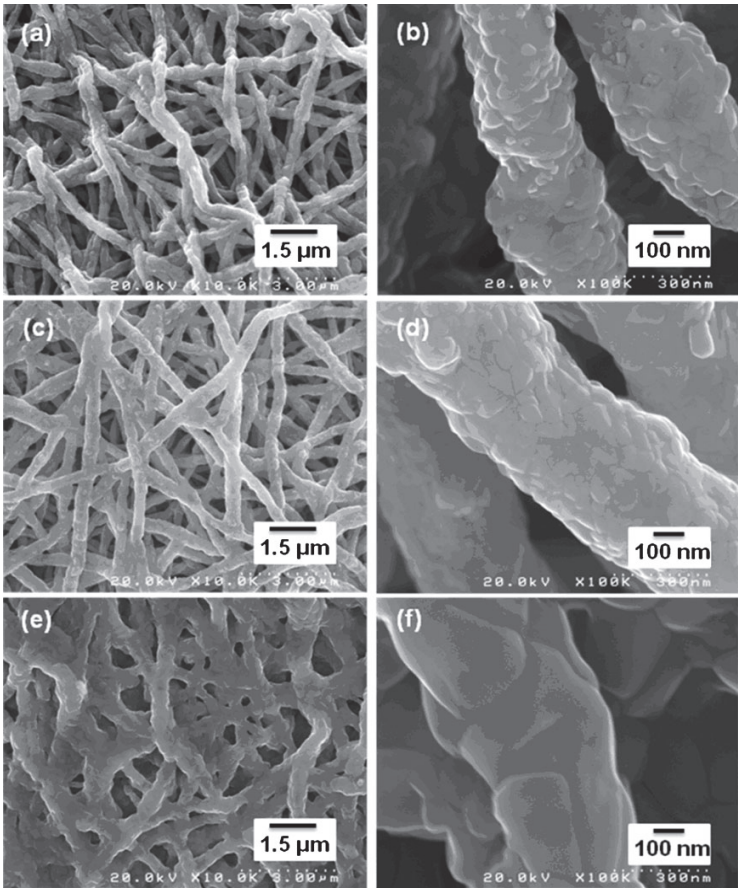

Fig. 7. FE-SEM images of Cu/Ni metallized (9:1, in deposition thickness) nanofibers annealed at 400 °C for (a, b) 6 h, (c, d) 12 h, and (e, f) 24 h.

and (220) reflections, for pure Ni crystals,[39] respectively. On the other hand, after annealing of Cu/Ni deposited nanofibers at higher temperature, such as 400 and 600 °C (Figs. 8c and 8d), new crystalline peaks were observed at 2θ = 32.5, 35.5, 38.7, 48.7, 53.4, and 58.5, corresponding to the (110), (002), (111), (202), (020), and (202) reflections, for CuO cubic crystals,[40] and 2θ = 37.3, 43.4, 63.0, 75.5, and 79.6, corresponding to the (111), (200), (220), (311), and (222) reflections, for NiO cubic crystals, respectively.[41, 42] The results suggested the transformation of pure metals to metallic oxides (CuO, NiO) during annealing processing. Specifically, in case of annealing temperature at 250 °C, different crystalline peaks were observed presumably due to the formation of intermediate metal oxide crystals (Cu_2O), which is however not clear at present. Fig. 9 shows WAXD patterns of Cu/Ni metallized (4:6, in deposited thickness) nanofibers before annealing (a) and after annealing at 250 °C (b), 400 °C (c), and 600 °C (d) for 12 h. The similar microstructures corresponding to metallic oxides (CuO, NiO) were also observed at the composition ratio of Cu/Ni=4:6 in deposited thickness.

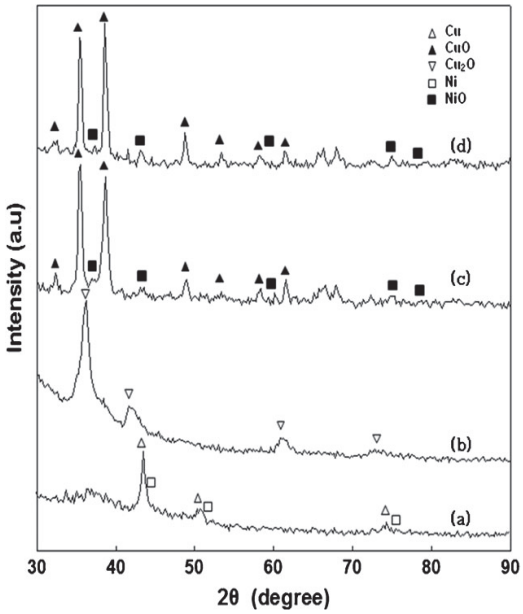

Fig. 8. WAXD patterns of Cu/Ni metallized (9:1, in deposited thickness) nanofibers before annealing and after annealing at 250 °C (b), 400 °C (c), and 600 °C (d) for 12 h.

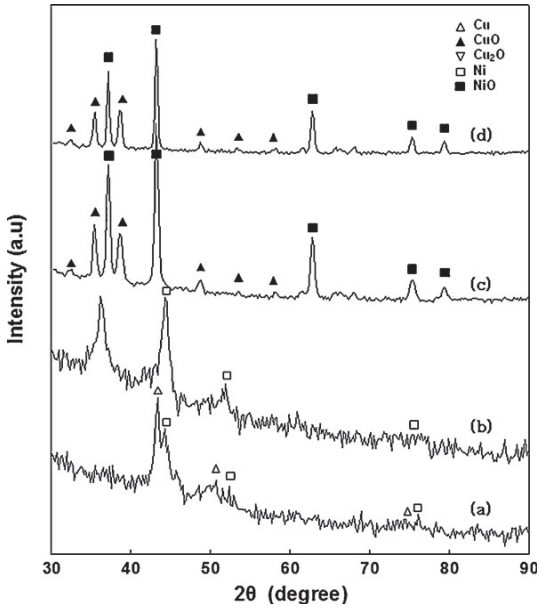

Fig. 9. WAXD patterns of Cu/Ni metallized (4:6, in deposited thickness) nanofibers before annealing (a) and after annealing at 250 °C (b), 400 °C (c), and 600 °C (d) for 12 h.

4. Mechanical properties of metallized nanofibers

4.1 Mechanical properties of metallized PU nanofiber webs

Stress–strain curves of pure PU nanofiber and metallized hybrid PU nanofiber webs are shown in Fig. 10. For all curves, stress–strain behavior shows a typical characteristic of thermoplastic elastomers, in that the stress–strain behaviors show a linear elasticity as their intrinsic materials' properties. Compared with pure PU nanofiber webs (Young's modulus 3.59 MPa), Young's modulus of metallized nanofiber webs was increased to 3.74 and 5.97 MPa for the metallized hybrid PU nanofiber webs with different copper layers of 10 and 100 nm, attributed to the metal hard-coating layers deposited on the nanofibers, which makes it a solid metal fiber resulting in an enhanced stiffness as well as conductivity. This result is crucial from an industrial point of view. Accordingly, the elongation of metallized nanofibers' webs decreases as the thickness of copper layer increases, suggesting that the elasticity of metallized hybrid nanofibers was reinforced by metallization: breaking elongation of metallized hybrid PU nanofiber webs decreased from 286% for pure PU nanofiber webs up to 131% for metallized hybrid PU nanofiber webs with the copper layer of 100 nm. On the other hand, the tensile strength of metallized nanofiber webs slightly decreased to 7.75 MPa for metallized hybrid PU nanofiber webs with the copper layer of 100 nm, compared with pure PU nanofiber webs (9.11 MPa).

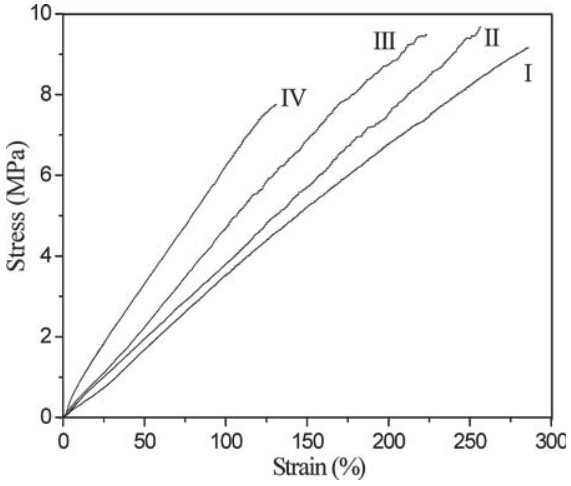

Fig. 10. Stress–strain curves of pure PU nanofiber web (I) and metalized PU nanofiber webs with different copper layers of 10 nm (II), 50 nm (III), and 100 nm (IV) at room temperature.

The detailed data are shown in Table 1. It can be, therefore, considered that the strength and ductility of electrospun nanofiber webs after metallization are greatly modified. The toughness, defined as the energy absorbed by the electrospun nanofiber webs until breaking, for metalized hybrid PU nanofiber webs with the copper layer of 100nm has the lower value (~0.010 J) than that of pure PU nanofiber webs (~0.026 J), suggesting that the higher amounts of the deposited copper layer onto PU nanofiber webs resulted in higher stiffness of metallized PU nanofiber webs. Although the decreased tensile strength behaviors of metallized hybrid nanofiber webs specifically with the copper layer of 100 nm are not fully understood, it could be considered that non-uniformly deposited thicker

copper layer may result in an easier deformation via small cracks or other imperfects in the metallized hybrid PU nanofibers, and thereby give rise to a poor tensile strength.

	Tensile modulus (MPa)	Tensile strength (MPa)	Elongation at break (%)
Pure PU	3.59	9.11	286
10 nm	3.74	9.64	256
50 nm	4.35	9.49	226
100 nm	5.97	7.75	131

Table 1. Mechanical properties of pure and Cu-deposited PU nanofibers with different thickness of the metal layers webs.

4.2 Mechanical properties of single metallized nanofibers

The mechanical properties of single metallized nanofibers were investigated by using recently developed tensile test machine [37, 43-44]. Evaluating the mechanical properties for the single nanofiber had remained lots of problems to be figured out. Limited reports have been made so far with special methods. The development of a novel method is required to study the mechanical properties of single nanofibers. For determining the tensile properties of single nanofibers, we specially developed the test machine (FITRON NFR-1000, RHESCA Co., Japan, [43], Fig. 11). It was demonstrated that the test machine is well operated for measurement of mechanical properties of nano/micro-sized fibers. Sample frame for collecting a single nanofiber is shown in Fig. 12. Oriented nanofibers between two parallel metal templates were collected while several single fibers were also collected on paper cutting sheet (as show in Fig. 12a), the nanofibers which cross over each other were eliminated under microscope (Fig. 12b). The cutting sheet with chosen single nanofiber was fixed on the holder (Fig. 12c). After a suitable fiber is selected and pasted with adhesive on a sample holder, the fiber axis is precisely set to align the stress axis of the holder using an optical microscopy. The main specifications of the developed system are as follows: the maximum loading capacity; 500 mN, the stroke; 20 mm, the loading speed; 5 - 20 μm/s, the displacement sensitivity; 1.0 μm, loading sensitivity; 1.0 μN, etc. Three parameters were determined from each stress–strain curve: Young's modulus, tensile strength, and elongation at break.

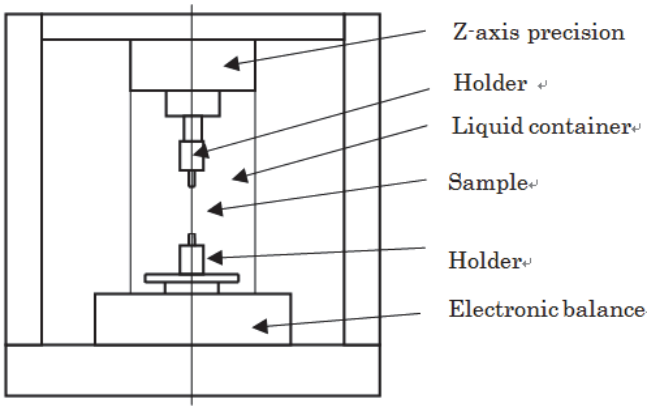

Fig. 11. Specially developed tensile test machine.

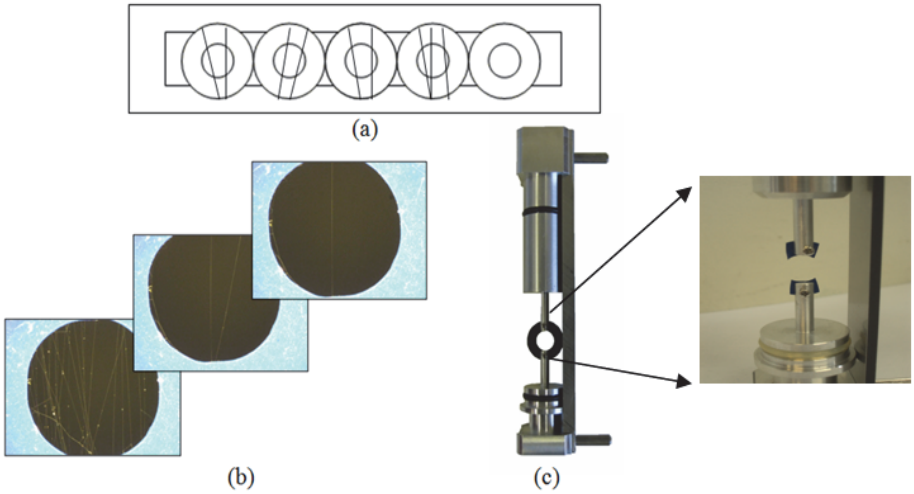

Fig. 12. Sample preparation, (a) Sample frame for collecting a single nanofibers, (b) single nanofibers preparation, (c) cutting sheet holder.

The tensile strength of pure PU, 30 and 50 nm Cu-deposited single PU nanofibers were also carried out at room temperature and the result was shown in Fig. 13. As seen in Fig. 13, the tensile strength of the Cu-deposited PU single nanofibers were increased with increasing the thickness of deposited copper layer. Compared to pure PU nanofibers, Young's modulus for the Cu-deposited PU nanofibers with the copper layers of 30 and 50 nm were increased to 610 and 750 MPa, respectively, due to the formation of metallic hard-coating layers onto the surface of PU nanofibers.[37] The detailed data were summarized in Table 2.

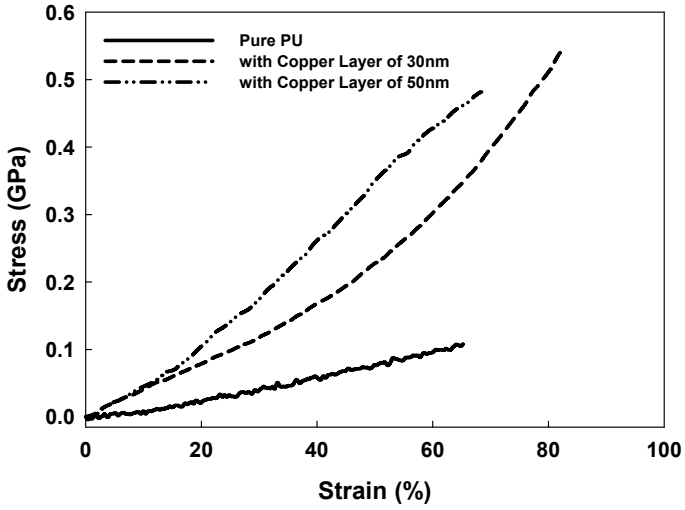

Fig. 13. Stress–strain curves of pure PU (solid line), 30 nm Cu-deposited (dotted line), and 50 nm deposited (dash-dot-dot line) single nanofibers (load: 10 mN, loading speed: 10 mm s^{-1}).

	Tensile modulus (MPa)	Tensile strength (MPa)	Elongation at break (%)
Pure PU	0.17	0.11	65.2
30 nm	0.61	0.54	82.0
50 nm	0.75	0.48	68.4

Table 2. Mechanical properties of pure PU single nanofiber and Cu-deposited PU single nanofiber with different thickness of the metal layers.

Here, we also report the tensile strength of various metals (for instance, Cu, Ni, Sn, and Al)-deposited PU nanofibers and various polymeric nanofibers measured by this recently developed tensile test machine. As previous said, we found that the tensile strength of metal-deposited PU single nanofibers was increased with increasing the thickness of deposited Cu layer.[37] Fig. 14 shows typical stress–strain curves of Cu-deposited (dash-dot line), Ni-deposited (medium dash line), Sn-deposited (solid line), Al-deposited (dotted line), and pure (dash-dot-dot line) single PU nanofibers (load: 10 mN, loading speed: 15 μm s^{-1}). In this work, the thickness of each metal layer was controlled and fixed to be about 50 nm. As seen in Fig. 14, compared with pure PU nanofibers (Young's modulus 170 MPa), mechanical properties of metal-deposited PU nanofibers were significantly increased and affected by the types of metals used for metallization. For instance, Young's modulus (8.81 GPa) of the Ni-deposited PU nanofibers was higher than those (Al-deposited, 1.0 GPa; Sn-deposited, 0.5 GPa; Cu-deposited, 1.9 GPa) of Al-, Sn-, and Cu-deposited PU nanofibers. On the other hand, among the metal-deposited PU nanofibers, Cu-deposited PU nanofibers showed the highest tensile strength and higher elongation at break, which resembles strong and tough thermoplastic properties. Although this is not fully understood, this can be considered due to the formation of polymer–metal nanocomposite layer in the interface areas of organic nanofibers and metallic layers.

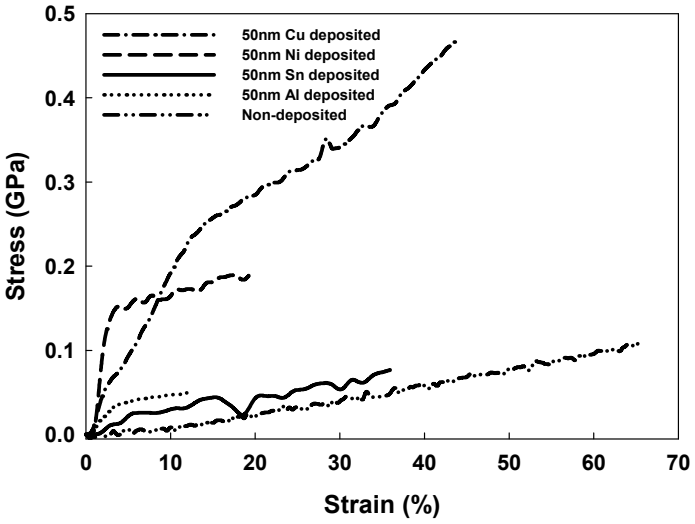

Fig. 14. Stress–strain curves of Cu-deposited (dash-dot line), Ni-deposited (medium dash line), Sn-deposited (solid line), Al-deposited (dotted line), and pure (dash-dot-dot line) single PU nanofibers (load: 10 mN, loading speed: 15 mm s^{-1}).

4.3 Electromagnetic interference (EMI) shield effects of metallized nanofiber webs

Shielding effectiveness (SE) is the ratio or impinging energy to the residual energy. When an electromagnetic wave pass through a shielding material, absorption and reflection takes place. Residual energy is part of the remaining energy that is neither absorbed nor reflected by the shielding material but it is emerged out from the shielding material. All electromagnetic waves consist of two essential components, a magnetic field (*H*) and electric field (*E*). These two fields are perpendicular to each other and the direction of wave propagation is at right angles to the plane containing the two components. The shielding should be in high conductance, thus metals, such as steel, copper, aluminum, etc., are the most common materials used for EMI shielding. However, metal shields have the inconvenience of poor mechanical flexibility, exceedingly high weight, propensity to corrosion, and limited tuning of the SE, while polymers offer lightness, low cost, easy shaping, etc [45]. Thus, polymer composites with discontinuous conducting fillers, such as metal particles, carbon particles, carbon fiber, are extensively employed in EMI shielding [46,47]. Among them, it is expected that the fiber with the high aspect ratio enables the formation of a conductive pathway through the resin matrix at low concentration. Fig. 15 shows the EMI SE (a) and the volume resistivity (b) of metal (Cu)-deposited nanofiber webs as a function of the thickness of metal layer. As can be seen in Fig. 15a, the EMI SE of metal-deposited nanofibers increased with increase in the thickness of deposited metal layer. The increase in EMI SE can be ascribed to the decrease in the electrical resistivity of metal-deposited nanofibers.[48]

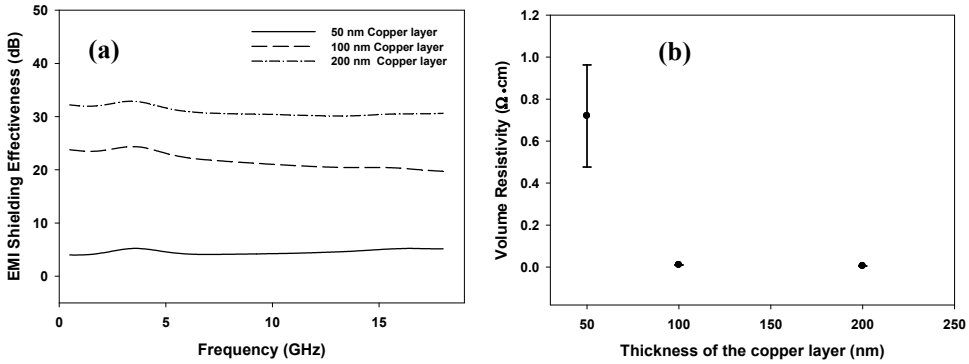

Fig. 15. EMI SE (a) and volume resistivity (b) of copper-deposited nanofiber webs as a function of the thickness of deposited Cu layer.

5. Summary

The design and development of electrospun fibers with sub-micrometer diameters from various kinds of materials has gained significant attention due to their large potential for manifold applications in electronics, optics, medicine, sensors, separation, storage, and so forth [49, 50]. The polymer fibers with sub-micrometer diameters down to a few nanometers can be prepared by electrospinning, which is a quick and facile technique to create high-surface-area fiber membranes where the fibers are several orders of magnitude smaller than those produced by conventional spinning techniques [51]. In this chapter, we have shown that the metallized nanofibers could be successfully prepared by using a combined

technology of electrostatic spinning and metallization. The electrospun nanofibers were metallized with different thicknesses of metal layer via a metallization. The tensile strength of the metal-deposited single nanofibers was investigated by recently developed tensile test machine. As a result, it was found that the tensile strength of 50 nm metal-deposited single nanofibers was dramatically improved, and was higher than that of pure polymer single nanofibers, which is attributed to the formation of metallic hard-coating layers onto the surface of single nanofibers. Moreover, the tensile strength of the metal-deposited single nanofibers was also depended on the types of metals (Cu, Ni, Sn, and Al) used for metallization. We have furthermore investigated the annealing behavior of Cu/Ni deposited nanofibers to find out optimum conditions enabling to prepare the metal alloy nanofibers. Certainly, based on the combined technology of electrospinning and metallization, the broad organic and metallic components should be adjustable, which will accelerate new applications, such as EMI SE, of these interesting conductive nanofiber webs. Furthermore, the procedures and costs could be reduced, which is, therefore, a promising straightforward technique for a large-scale production of novel metallized hybrid nanofiber webs.

6. References

[1] A. C. Patel, S. Li, C. Wang, W. Zhang, Y. Wei, *Chem. Mater.* 19, 1231 (2007).
[2] M. K. Shin, S. S. Kim, S. J. Kim, S. K. Kim, H. Kee, *Appl. Phys. Lett.* 88, 193901 (2006).
[3] D. Christopher, L. Xin, Z. David,W. Xianyan, F. B. Ferdinando,W. James, A. S. Lynne, K. Jayant, *Nano Lett.* 3, 143 (2003).
[4] Y. Ji, B. Li, S. Ge, J. C. Sokolov, M. H. Rafailovich, *Langmuir* 22, 1321 (2006).
[5] S. D. McCullen, D. R. Stevens, W. A. Roberts, S. S. Ojha, L. I. Clarke, R. E. Gorga, *Macromolecules* 40, 997 (2007).
[6] K. Wei, J. H. Xia, B. S. Kim, I. S. Kim, *J. Polym. Res.* DOI: 10.1007/s10965-010-9451-z.
[7] C. K. Kim, B. S. Kim, F. A. Sheikh, U. S. Lee, M. S. Khil, H. Y. Kim, *Macromolecules* 40, 4823 (2007).
[8] S. R. Davis, A. R. Brough, A. J. Atkinson, *J. Non-Cryst. Solids* 315, 197 (2003).
[9] D. K. Chattopadhyay, K. V. SN. Raju, *Prog. Polym. Sci.* 32, 352 (2007).
[10] [10] R. A. Caruso, J. H. Schattka, A. Greiner, *Adv. Mater.* 13, 1577 (2001).
[11] [11] H. Hou, J. J. Ge, J. Zeng, Q. Li, D. H. Reneker, A. Greiner, S. Z. D. Cheng, *Chem. Mater.* 17, 967 (2005).
[12] A. C. Patel, S. Li, J. M. Yuan, Y. Wei, *Nano Lett.* 6, 1042 (2006).
[13] Z. Sun, E. Zussman, A. L. Yarin, J. H. Wendorff, A. Greiner, *Adv. Mater.* 15, 1929 (2003).
[14] A. V. Bazilevsky, A. L. Yarin, C. M. Megaridis, *Langmuir* 23, 2311 (2007).
[15] H. W. Jun, V. Yuwono, S. E. Paramonov, J. D. Hartgerink, *Adv. Mater.* 17, 2612 (2005).
[16] Z. M. Huang, Y. Z. Zhang, M. Kotaki, S. Ramakrishna, *Compos. Sci. Technol.* 63, 2223 (2003).
[17] D. Li, Y. Xia, *Adv. Mater.* 16, 1151 (2004).
[18] A. Formhals, US Patent 1975504, 1934.
[19] K. O. Kim, Y. A Seo, B. S. Kim, K. J. Yoon, M. S. Khil, H. Y. Kim, I. S. Kim, *Colloid & Polymer Science* 289, 863 (2011).
[20] N. Kimura, H. K. Kim, B. S. Kim, K. H. Lee, I. S. Kim, *Macromol. Mater. & Eng.* 295, 1090 (2010).

[21] H. Sato, K. O. Kim, H. K. Kim, B. S. Kim, Y. Enomoto, I. S. Kim, *Fibers and Polymers* 11, 1123 (2010).
[22] Q. B. Yang, D. M. Li, Y. L. Hong, Z. Y. Li, C. Wang, S. L. Qiu, Y. Wei, *Synth. Met.* 137, 973 (2003).
[23] M. F. Ottaviani, R. Valluzzi, L. Balogh, *Macromolecules* 35, 5105 – 5115 (2002).
[24] M. Bognitzki, H. Hou, M. Ishaque, T. Frese, M. Hellwig, C. Schwarte, A. Schaper, J. H. Wendorff, A. Greiner, *Adv. Mater.* 12, 637 (2000).
[25] Q. Peng, X. Y. Sun, J. C. Spagnola, G. K. Hyde, R. J. Spontak, G. N. Parsons, *Nano Lett.* 3, 719 (2003).
[26] K. Wei, T. Ohta, B. S. Kim, K. W. Kim, K. H. Lee, M. S. Khil, H. Y. Kim, I. S. Kim, *Polym. Adv. Technol.* 21, 746 (2010).
[27] H. R. Kim, T. Ito, B. S. Kim, Y. Watanabe, I. S. Kim, *Adv. Eng. Mater.* 13, 376 (2011).
[28] J. C. Park, T. Ito, K. O. Kim, K. W. Kim, B. S. Kim, M. S. Khil, H. Y. Kim, I. S. Kim, *Polym. J.* 42, 273 (2010).
[29] I. S. Kim, K. Wei, T. Ohta, B. S. Kim, Y. Watanabe, *Materials Science Forum 638-642*, 1719 (2010).
[30] O. Ohsawa, K. H. Lee, B. S. Kim, S. Lee, I. S. Kim, *Polymer* 51, 2007 (2010).
[31] K. Kim, M. Yu, X. Zong, J. Chiu, D. Fang, Y. S. Seo, B. S. Hsiao, B. Chu, M. Hadjiargyrou, *Biomaterials* 24, 4977 (2003).
[32] S. H. Tan, R. Inai, M. Kotaki, S. Ramakrishna, *Polymer* 46, 6128 (2005).
[33] J. H. Park, B. S. Kim, Y. C. Yoo, M. S. Khil, H. Y. Kim, *J. Appl. Polym. Sci.* 107, 2211 (2008).
[34] G. Carotenuto, *Appl. Organomet. Chem.* 15, 344 (2001).
[35] Z. Li, H. Huang, C. Wang, *Macromol. Rapid Commun.* 27, 152 (2001).
[36] ASM Handbook, ASM International, Metals Park, OH 1992, p. 5.
[37] H. R. Kim, N. Kimura, H. S. Bang, B. S. Kim, Y. Watanabe, I. S. Kim, *Mater. Sci. Forum* 654-656, 2463 (2010).
[38] Z. Li, H. Huang, C. Wang, *Macromol. Rapid Commun.* 27, 152 (2006).
[39] N. A. M. Barakat, B. S. Kim, H. Y. Kim, *J. Phys. Chem. C* 113, 531 (2009).
[40] S. Asbrink, A. Waskowska, *J. Phys. : Condens. Matter*. 3, 8173 (1991).
[41] I. Hotovy, J. Huran, L. Spiess, *J. Mater. Sci.* 39, 2609 (2004).
[42] H. Qiao, Z. Wei, H. Yang, L. Zhu, X. Yan, *J. Nanomater.* 2009, 1 (2009).
[43] I. S. Kim, Y. Enomoto, T. Takahashi, *Sen'i Gakkaishi* 65, 325 (2009).
[44] K. Wei, J. H. Xia, Z. J. Pan, G. Q. Chen, B. S. Kim, I. S. Kim, *Advanced Materials Research* 175-176, 294 (2011).
[45] J. M. Thomassin, C. Pagnoulle, L. Bednarz, I. Huynen, R. Jerome, C. Detrembleur, *J. Mater. Chem.* 18, 792 (2008).
[46] M. S. P. Shaffer, A. H. Windle, *Adv. Mater.* 11, 937 (1999).
[47] T. Makela, J. Sten, A. Hujanen, H. Isotalo, *Synth. Met.* 101, 707 (1999).
[48] M. H. Al-Saleh, U. Sundararaj, *Carbon* 47, 1738 (2009).
[49] M. Bognitzki, M. Becker, M. Graeser, W. Massa, J.H. Wendorff, A. Schaper, D. Weber, A. Beyer, A. Golzhauser, A. Greiner, *Adv. Mater.* 18, 2384 (2006).
[50] R. Dersch, M. Steinhart, U. Boudriot, A. Greiner, J.H. Wendorff, *Polym. Adv. Tech.* 15, 276 (2005).
[51] C. Drew, X. Liu, D. Ziegler, X. Wang, F.F. Bruno, J. Whitten, L.A. Samuelson, J. Kumar, *Nano Lett.* 3, 143 (2003).